The stability and electro-oxidation of carbon monoxide on model electrocatalysts: Pt(1 1 1)–Sn(2 × 2) and Pt(1 1 1)–Sn($\sqrt{3} \times \sqrt{3}$)R30°

Brian E. Hayden*, Michael E. Rendall, Oliver South

School of Chemistry, University of Southampton, Southampton SO17 1BJ, UK

Available online 28 November 2004

Abstract

The surface redox behaviour, the stability, and the electro-oxidation of CO on model platinum–tin surface alloy catalysts has been studied by ex situ electrochemical measurements. The Pt(1 1 1)–Sn(2 × 2) and Pt(1 1 1)–Sn($\sqrt{3} \times \sqrt{3}$)R30° surfaces have been prepared and characterised in UHV by vapour deposition of Sn on Pt(1 1 1) and the surfaces subsequently transferred for electrochemical investigation. A surface redox couple, which is associated with the adsorption/desorption of hydroxide on the Sn sites, is observed at $0.28\,V_{RHE}/0.15\,V_{RHE}$ in H_2SO_4 electrolyte on both surfaces. Evidence that it is associated with the adsorption of OH comes from ex situ photoemission measurements, which indicate that the Sn atoms are in a metallic state at potentials below $0.15\,V_{RHE}$, and an oxidised state at potentials above 0.28_{RHE}. Specific adsorption of sulphate anions is not associated with the surface process since there is no evidence from photoemission of sulphate adsorption, and the same surface couple is observed in $HClO_4$ electrolyte. A second surface redox couple, associated with further oxidation of the Sn sites in the alloy surfaces, is observed at $0.8\,V_{RHE}/0.58\,V_{RHE}$. CO is adsorbed from solution at 300 K, with saturation coverages of $0.37 \pm 0.05\,ML$ and $0.2 \pm 0.05\,ML$, respectively. The adsorbed CO is oxidatively stripped at the potential coincident with the adsorption of hydroxide on the tin sites at the lower potential of $0.28\,V_{RHE}$. This strong promotional effect is unambiguously associated with the bi-functional mechanism. The Sn induced activation of water, and promotion of CO electro-oxidation, is sustained as long as the alloy structure remains intact, in the potential range below $0.5\,V_{RHE}$. The instability of the alloy surface at higher potentials is associated with the second redox couple. The redox behaviour at higher potentials is modified by the presence of CO in stripping experiments, with couples now observed at $0.78\,V_{RHE}/0.56\,V_{RHE}$, and $0.9\,V_{RHE}/0.70\,V_{RHE}$. This behaviour may be associated with enhanced oxidation through the exclusion of sulphate anions at the surface by CO.
© 2004 Elsevier B.V. All rights reserved.

Keywords: Electrocatalysis; Alloy; CO oxidation; Fuel cell; Ex situ

1. Introduction

The promotion of CO electro-oxidation at low over-potentials on platinum surfaces can provide the CO tolerance required of anode catalysts in reformate fuelled PEM fuel cells [1]. Such promoted surfaces may also provide active catalysts for the direct oxidation of methanol in Direct Methanol PEM [2] fuel cells, since CO is a potentially poisoning intermediate in the surface reaction. The alloying of a second, or even third, metal component in platinum has been the favoured method of providing CO-tolerant anode catalysts, and to date the most active catalytic system for both applications is the Pt/Ru alloy [3]. The mechanism by

which the Ru component of the alloy affords CO tolerance has been investigated in a number of studies of CO oxidation at well-characterised surfaces of Pt/Ru bulk polycrystalline alloys [4–6], and ruthenium modified single crystal platinum surfaces [7–12]. The adsorption and reaction of CO on Pt/Ru has also been the subject of kinetic modelling [13,14] and ab initio calculation [15–17]. The results suggest that the promotion of CO electro-oxidation through the activation of water by the ruthenium component in the surface (to provide the oxidant in a bi-functional mechanism), or an electronic effect of Ru on Pt ensuring lower mean coverages of CO, are two possible mechanisms by which CO tolerance is afforded.

The Pt/Sn alloy system has been suggested to be a potential alternative CO-tolerant PEM, and DMFC, anode electro-catalyst, since it was suggested to exhibit superior characteristics even to the Pt/Ru alloy for methanol oxidation

* Corresponding author. Tel.: +44 2380 592776; fax: +44 2380 598326.
 E-mail address: beh@soton.ac.uk (B.E. Hayden).

[18–20]. The mechanism by which the activity was induced by the Sn was suggested to be a result of an electronic (ligand) effect of the Sn on the CO promoting its oxidation [18,19]. Since then the promoting mechanism has been the subject of considerable debate (see [21] and references therein), and is complicated by the possible influence of Sn on the dehydrogenation reaction in addition to the removal of the CO intermediate. A series of experiments of well-characterised surfaces of Sn modified Pt, Pt/Sn, single crystal surfaces provides a considerable insight regarding the influence of Sn in CO [22–25] and methanol [23,26] oxidation. It was found that methanol oxidation was not promoted by Sn on the surface, but could be promoted by a solution phase redox couple involving Sn. It was also concluded that steady state CO electro-oxidation was indeed promoted by Sn at the surface. However, the adsorption and stripping experiments suggested that not all CO was oxidised at low potential, and it was concluded that it must be the remaining CO that dominated the kinetics of methanol oxidation.

Recently, the promotion of CO electro-oxidation by islands of UPD Sn on Pt(1 1 1) was again explained by an electronic perturbation of the CO [27], and indeed a slight weakening of the Pt–CO bond is also evidenced in TPD measurements made on the ordered Pt(1 1 1)–Sn alloy surfaces [28]. The originally proposed ligand effect [18,19] was partly substantiated by the absence of a surface redox couple that could account for CO electro-oxidation at low potentials. The redox couple, associated with UPD [29] and spontaneously deposited [30] Sn, is observed at $0.6_{RHE}/0.56_{RHE}$ on Pt(1 1 1). Nevertheless it is suggested [31] that a surface Sn^{2+} species is active in the electro-oxidation CO, and intermediates associated with the oxidation of methanol and formic acid.

We have employed metal vapour deposition (MVD) of Sn on the Pt(1 1 1) surface to produce two well ordered surface alloys of Pt/Sn [28,32,33], Pt(1 1 1)–Sn(2×2) with $\theta_{Sn} = 0.25$, and Pt(1 1 1)–Sn($\sqrt{3} \times \sqrt{3}$)R30° with $\theta_{Sn} = 0.33$. These well defined model Pt/Sn alloy surfaces have been used to investigate the surface redox behaviour of the Sn, and specifically its ability to activate water [34]. We show that the activation of water to produce adsorbed hydroxide takes place at very low over-potential, significantly lower than the Sn^{2+}/Sn^{4+} couple, which gives rise to oxidative dissolution of the Sn. Importantly, we also show unambiguously that the CO electro-oxidation on such surfaces takes place coincidentally with the activation of water by the Sn site. This provides direct evidence that promotion takes place by provision of the oxidant at low over-potential through a bi-functional mechanism.

The results [34] while consistent with the observed activities of PtSn alloys in CO oxidation exhibit some differences in the details of the cyclic voltammetry of the bulk $Pt_3Sn(1 1 1)$ surface [24,25,31]. The latter also exhibits significant structural changes continuously to relatively high potentials [35], where the surface is reported to be stable. The results presented here indicate that in the case of the Pt(1 1 1)–Sn surface alloy structures, the surface is quite unstable at relatively modest oxidising potentials.

2. Experimental

Experiments have been conducted in a UHV electrochemical transfer system that consists of two independent UHV chambers; a surface analysis chamber and an electrochemical chamber, the basic design of which has been described elsewhere [36,37]. The single crystal is mounted on the end of a long-travel magnetic manipulator which allows for rapid transfer between the two chambers. The sample is prepared and characterised in the analysis chamber using X-ray photoelectron spectroscopy (XPS), low energy ion scattering spectroscopy (LEISS), low energy electron diffraction (LEED), and temperature programmed desorption (TPD). The combination of these techniques combined with metal vapour deposition (MVD) was used to prepare and characterise the surface alloys of Pt(1 1 1)–Sn.

The UHV transfer system allows the single crystal to be moved from the analysis chamber into the electrochemical chamber, the gate valve closed, and the electrochemical chamber raised to an atmosphere of dry argon. A glass electrochemical cell is raised to allow contact of the electrolyte with the modified crystal under potential control. The two chambers have independent pumping systems allowing the crystal to be returned to the surface analysis chamber after electrochemical investigation.

The MVD Sn source was a resistively heated tantalum boat Knudsen cell containing pure tin wire (+99.99%, Goodfellow) with the temperature of the source measured with a Chromel–Alumel thermocouple. Tin was deposited at a boat temperature of 800 K and a deposition rate of ca. $0.05 \, ML \, min^{-1}$ as monitored by in situ X-ray photoelectron spectroscopy by applying the appropriate sensitivity factors [38]. The tin was incorporated into the surface to form the alloy phases by flash annealing the platinum crystal to 1000 K [28]. The surface coverage of tin was monitored by low energy ion scattering spectroscopy, and the formation of the ordered over-layer by low energy electron diffraction. Electrochemistry was performed using a glass cell, after raising the pressure of the antechamber, to which the sample was transferred, to atmospheric pressure of oxygen-free argon. The electrolyte was $0.5 \, M \, H_2SO_4$ or $0.5 \, M \, HClO_4$, and a Pd/H_2 couple used as reference electrode. All solutions were made using ultra-pure (Millipure) water (conductivity $> 18 \, M\Omega^{-1} \, cm^{-2}$).

3. Results and discussion

3.1. Pt(1 1 1)–(2 × 2) Sn and Pt(1 1 1)–(√3 × √3)R30° Sn surfaces

There are a number of ordered surface structures that can be formed by the deposition of tin on the Pt(1 1 1) surface [28,32,33,39] dependant on the surface temperature and the coverage of tin. To form the ordered surface alloys, the crystal is annealed after the initial tin deposition. To form surface

alloys that extend across the entire surface (as inferred from LEED measurements) approximately 5 ML of tin was deposited at 300 K. The surface was subsequently annealed to 1000 K for 10 s to initiate the surface rearrangement. The reason for the seemingly excess amount of tin is due to a large proportion of the tin vaporising from the surface into the vacuum rather than becoming incorporated into the surface.

The two ordered alloys that were prepared for the electrochemical investigations were the Pt(1 1 1)–Sn(2 × 2) and the Pt(1 1 1)–Sn($\sqrt{3} \times \sqrt{3}$)R30° surfaces with coverages of $\theta_{Sn} = 0.25$ and 0.33, respectively. Fig. 1 shows the LEED patterns measured for the two alloys together with the reciprocal space structure, and the corresponding real space structures.

LEISS, LEED and XPS were used to characterise the surface alloys. It was evident that some Sn was incorporated in the second and third layer of the Pt(1 1 1) surface during alloy formation.

3.2. The electrochemical surface redox behaviour of the Pt/Sn alloy

Fig. 2A shows the cyclic voltammetry (CV) of the Pt(1 1 1) surface (broken line) and the Pt(1 1 1)–Sn(2 × 2) alloy surface
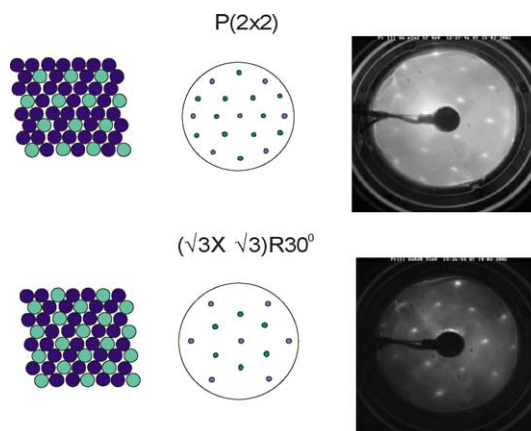

Fig. 1. LEED patterns (together with the reciprocal space structures) obtained for the Pt(1 1 1)–Sn(2 × 2) and Pt(1 1 1)–Sn($\sqrt{3} \times \sqrt{3}$)R30° surface alloys. The beam energies were 57 eV and 91 eV, respectively. A real space representation of the surfaces is also shown, with the incorporated Sn atoms shown as the lighter spheres.

(solid line), both in 0.5 M H_2SO_4 electrolyte, measured at a sweep rate of 100 mV s^{-1}. The Pt(1 1 1) "butterfly" structure is that expected for a clean and well ordered surface [40], exhibiting the reversible hydrogen and sulphate adsorption
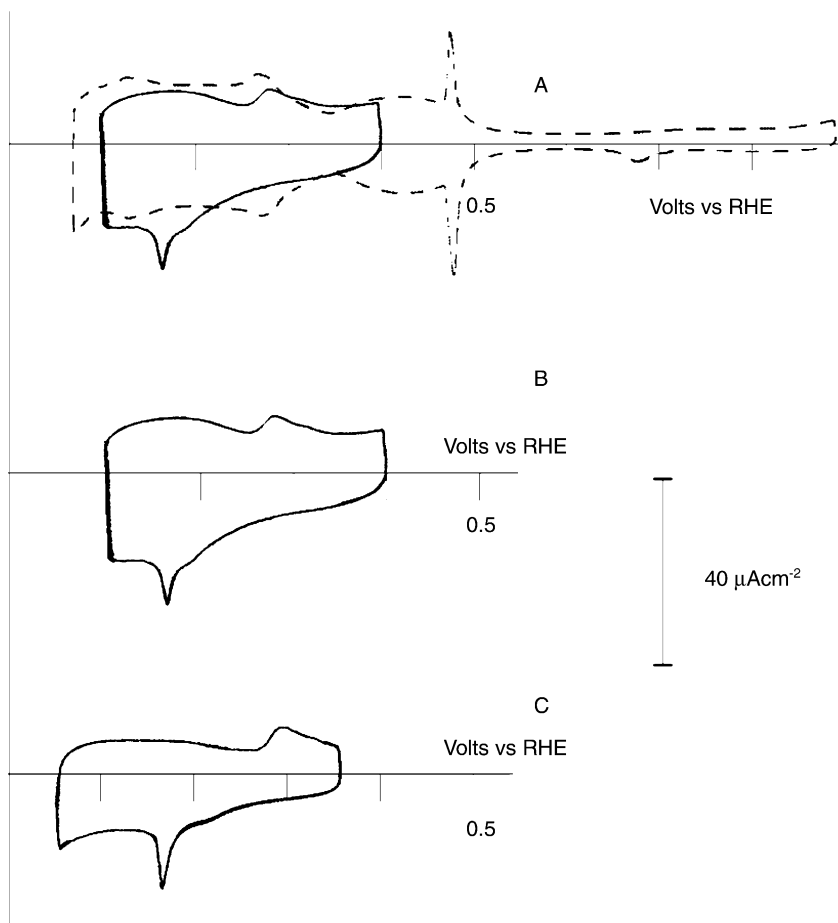

Fig. 2. (A) Cyclic volammograms of Pt(1 1 1) (dashed line) and Pt(1 1 1)–Sn(2 × 2) (solid line) surfaces in 0.5 M H_2SO_4. Cyclic volammograms of Pt(1 1 1)–Sn(2 × 2) (B) and Pt(1 1 1)–Sn($\sqrt{3} \times \sqrt{3}$)R30° (C) surfaces in 0.5 M H_2SO_4. The scan rate was 100 mV s^{-1}.

structure, the sharp long range ordering peaks at $0.48\,V_{RHE}$, and the sulphate/bisulphate structure above $0.6\,V_{RHE}$.

Superimposed on the Pt(1 1 1) voltammetry is the CV of the Pt(1 1 1)–Sn(2 × 2) Sn alloy surface (solid line). The CV shown was the first obtained following preparation of the Pt(1 1 1)–Sn(2 × 2) Sn structure in UHV, and transfer to the electrochemical cell, making contact under potential control at $0.05\,V_{RHE}$. The CV obtained does not change with subsequent cycling so long as the potential was not raised above ca. $0.5\,V_{RHE}$. The hydrogen UPD structure in the potential range of the measurement (e.g. the reversible peaks at ca. $0.26\,V_{RHE}$ associated with the defects originating from Pt(1 0 0) and Pt(1 1 0) step sites [40]) of the Pt(1 1 1) surface is largely destroyed by the presence of the Sn. However there remains an underlying pseudo-capacitance which we do associate with hydrogen adsorption on the alloy surface. The CV of the alloy surface exhibit small and relatively sharp peaks superimposed on the broadened double layer current in the anodic and cathodic scans at $0.28\,V_{RHE}/0.15\,V_{RHE}$, respectively. Current densities are given, but it should be noted that there is an absolute error of $\pm 10\,\mu A\,cm^{-2}$ since it was difficult to define the meniscus contact area on the face of the crystal since the incorporation of the Sn resulted in an observed strong wetting of the surface on contact. The peaks in the anodic and cathodic scans at $0.28\,V_{RHE}/0.15\,V_{RHE}$ are associated with a surface redox couple involving the adsorption and desorption of OH at the platinum sites.

Fig. 2B and C shows the CV of the two surface alloy structures Pt(1 1 1)–Sn(2 × 2) and Pt(1 1 1)–Sn($\sqrt{3} \times \sqrt{3}$)R30°, measured in H_2SO_4 electrolyte at a sweep rate of $100\,mV\,s^{-1}$. The associated LEED patterns and the real space structures for the alloys are shown in Fig. 1. LEED revealed that the ordered alloy was formed over the complete Pt(1 1 1) surface in both cases. The CV shown was the first measured on the transferred surfaces, and remained unaltered in further scans so long as the potential was not raised above ca. $0.5\,V_{RHE}$. Both surfaces exhibit the small and relatively sharp peaks superimposed on a broad double layer current in the anodic and cathodic scans at $0.28\,V_{RHE}/0.15\,V_{RHE}$ respectively which we associate with OH adsorption/desorption. The peaks are found at the same potential for the two alloy surfaces. The common potential for the couple is understandable if the associated process is the activation of water to produce adsorbed OH. This process will be dominated by the electronic response of the Sn atom in the Pt(1 1 1) surface. The local electronic structure of the Sn will be primarily influenced by the next nearest neighbours in the surface and in the second layer. The Sn atoms are surrounded by platinum next nearest neighbours in both surface alloy structures (Fig. 1). The difference in the next nearest neighbour concentration of Sn atoms appears to have little effect on the promoting Sn atom. DFT calculations indicate [41] that OH adsorption is relatively facile on Sn atoms rather than platinum atoms on a Pt$_3$Sn(1 1 1) model alloy due to a strong Sn-O interaction. The OH favours an a-top site on the Sn in Pt$_3$Sn (1 1 1)

rather than a HCP three-fold hollow site on bare platinum. The Sn atoms have been found to 'relax' out of the Pt$_3$Sn (1 1 1) surface into a p(2 × 2) pattern.

The possibility that the peaks could be due to the adsorption of sulphate rather than the adsorption of OH on tin was also considered. It has been recently established [35] on the bulk alloy crystal surface of Pt$_3$Sn(1 1 1)–(2 × 2) that (bi)sulphate adsorption occurs on the platinum component of the surface. An IR band at $1240\,cm^{-1}$ associated with the sulphate anion is observed to increase in intensity with increasing potential in the range $0.28 < V_{RHE} < 0.50$. It has also been suggested that there is an enhancement of anion adsorption to lower potentials by the addition of ad-metals to Pt(1 1 1) by other researchers [42,43]. This has been attributed to the local work function modification the presence of tin may have on the platinum. In early studies on the Pt$_3$Sn alloy surface [26] a reversible peak associated with the well ordered alloy surface was observed at $0.34\,V_{RHE}$ in H_2SO_4 electrolyte, and its persistence in 0.3 M HF electrolyte lead to the conclusion that it was not associated with sulphate anion adsorption. Later measurements on the same surface only suggest sulphate adsorption in H_2SO_4 [35].

There is strong evidence that the alloy induced peaks in the CV which we associate with OH adsorption/desorption (Fig. 2) are not associated with sulphate anion adsorption. Perhaps the most compelling is the result of carrying out the cyclic voltammetry of the alloy surface in electrolytes not containing the sulphate anion. Fig. 3 shows the result of measuring the CV of Pt(1 1 1)–Sn($\sqrt{3} \times \sqrt{3}$)R30° alloy surface in 0.5 M $HClO_4$ electrolyte. The results can be directly compared to those obtained in H_2SO_4 electrolyte (Fig. 2). Note that the same structure in the voltammetry, i.e. the surface redox couple at $0.27\,V_{RHE}/0.12\,V_{RHE}$ is observed. The alloy induced peaks in the voltammetry carried out in H_2SO_4 electrolyte are clearly not associated with sulphate adsorption. In addition, no sulphate adsorption is observed in ex situ photoemission experiments following transfer of the surface back to UHV after breaking contact at $0.4\,V_{RHE}$. It will also become evident that the underlying structure of the anodic peak remains in the presence of adsorbed CO. CO adsorp-

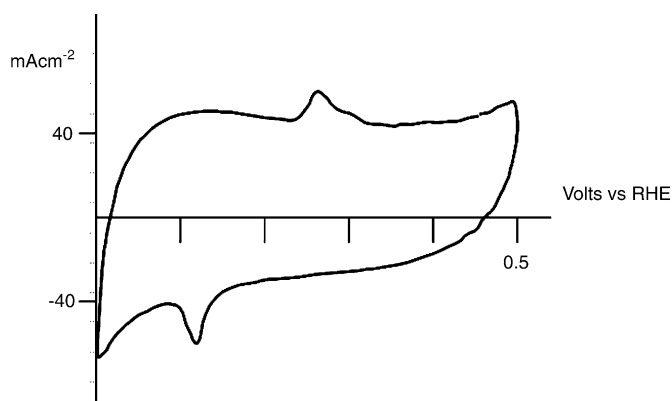Fig. 3. Cyclic volammogram of the Pt(1 1 1)–Sn($\sqrt{3} \times \sqrt{3}$)R30° (solid line) surface in 0.5 M $HClO_4$. The scan rate was $100\,mV\,s^{-1}$.

tion is known to strongly poison hydrogen adsorption and sulphate adsorption on platinum surfaces.

In order to confirm the change in oxidation state of the Sn associated with hydroxide adsorption, meniscus contact between the crystal and the electrolyte was broken at two potentials, 0.1 V_{RHE} and 0.4 V_{RHE}, above and below the potentials associated with the OH adsorption/desorption process, at 0.28 V_{RHE}/0.15 V_{RHE}, respectively (Fig. 2). This experiment was carried out on the Pt(1 1 1)–Sn($\sqrt{3} \times \sqrt{3}$)R30° alloy surface. In each case, the electrochemical antechamber was evacuated and the crystal immediately transferred back to the UHV chamber in order to carry out X-ray photoelectron spectroscopy. The results in the form of the Sn(3d) doublet are shown in Fig. 4. Fig. 4A shows a spectrum taken of the prepared Pt(1 1 1)–Sn($\sqrt{3} \times \sqrt{3}$)R30° alloy surface before transfer (dotted line), and a spectrum measured following emersion of the surface at 0.1 V_{RHE}. Note that before emersion, the surface had been previously cycled to 0.4 V_{RHE}. The results show that there is no significant change in the chem-
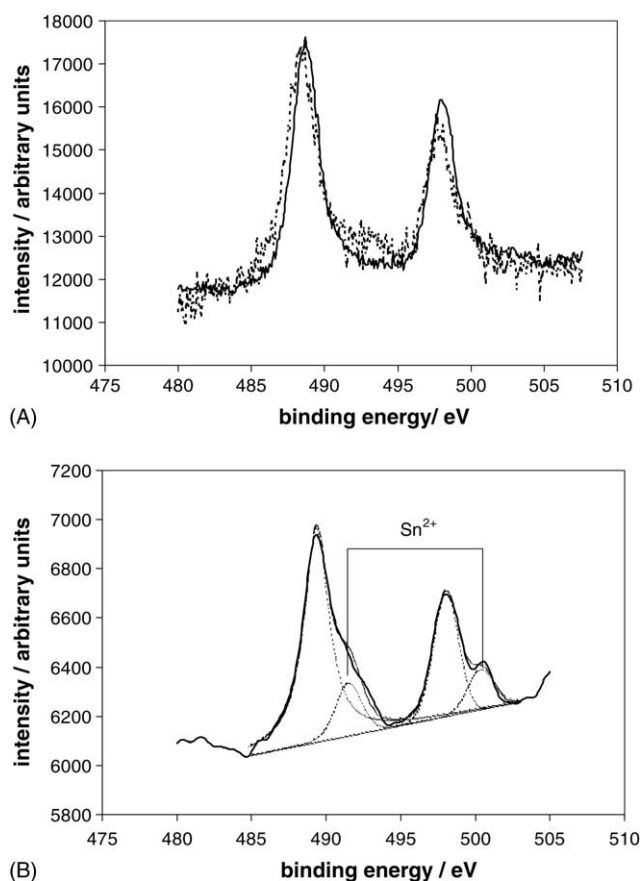

Fig. 4. X-ray photoelectron spectrum (Sn(3d) region) of the Pt(1 1 1)–Sn($\sqrt{3} \times \sqrt{3}$)R30° alloy surface (A) before transfer to the electrochemical cell (dotted line), and after emersion at 0.1 V_{RHE} following several cycles to 0.4 V_{RHE}, and transferring the surface back into the UHV chamber. (B) shows the a photoemission spectrum following emersion at 0.4 V_{RHE}. Following background subtraction, the measured spectrum (solid line) has been deconvoluted into the contributions of the Sn^0 and Sn^{2+} components (dotted lines), and the sum of these is shown (dashed line) for comparison with the original spectrum.

ical environment of the Sn, and that the Sn atoms remain in the same metallic state as that observed on preparation of the alloy in UHV. Fig. 4B shows the photoemission spectrum measured following emersion at 0.4 V_{RHE}. It is evident that there are two Sn chemical environments, one of which corresponds to that of $Sn^0(Sn(3d^{3/2}) = 489\,eV)$ and that of an oxidised Sn state which corresponds approximately to Sn^{2+} $(Sn(3d^{3/2}) = 492\,eV)$, using results of core level shifts of a variety of Sn compounds [38] to establish the Sn^{2+} oxidation state. Note that this ex situ measurement of the Sn oxidation state does not reflect directly the "in situ" oxidation state of the Sn following OH adsorption, since chemical reaction following transfer may result in some associative water formation, with oxygen remaining on the surface. However, the results presented in Fig. 4 do unambiguously indicate that the Sn atoms are in an oxidised state at potentials above the anodic peak at 0.28 V_{RHE}. Further the results indicate that this state does not correspond to Sn^{4+}, the state probably responsible for oxidative disruption of the alloy at higher potentials. One may have expected all Sn atoms in the top surface layer to have the oxidised state following OH adsorption and transfer to UHV and this is clearly not the case (Fig. 4B). However the XPS measurement includes part of the Pt(1 1 1) surface which has not made contact with the electrolyte. In addition, we find that a Sn concentration in the top four layers (measured at these kinetic energies in XPS) is required in order to establish a well formed ordered surface alloy structure. The un-oxidised Sn, therefore, associated with the area of the surface outside the meniscus contact area, and a component incorporated below the top surface layer. There is also the possibility of water formation during emersion and transfer which would also lead to some net reduction in the surface.

Recent X-ray diffraction measurements of the $Pt_3Sn(1 1 1)$–(2 × 2) surface structure [35] reveal significant extension of the Pt–Sn bond distance, and a relaxation of the Pt interlayer spacing, in the surface the potential region $0.05 < V_{RHE} < 0.55$. This potential region includes the potentials at which we are suggesting that OH adsorption takes place on the surface alloy structures. The large changes observed in the interlayer spacings are consistent with the adsorption of OH particularly in the light of DFT calculations which predict the extension of the Pt–Sn bond distance [41]. It is not clear, however, why the effective rumpling observed in XRD [35] takes place over a relatively wide potential range. We note that the sharp redox behaviour observed in these studies is not observed in the voltammetry of the $Pt_3Sn(1 1 1)$–(2 × 2) surface [24,25,31]. On the other hand, the reversible broad structure observed at 0.35 V_{RHE}, correlated with (bi)sulphate adsorption [35], is not observed on the surface alloy structures (Fig. 3). We can only suggest that this difference may be associated with either intrinsic differences between the behaviour of the surface generated at the termination of the bulk alloy and the surface alloy, or is associated with the extent of surface order.

Cycling the Pt(1 1 1)–Sn($\sqrt{3} \times \sqrt{3}$)R30° surface to higher potential in 0.5 M H_2SO_4 can lead to the oxidative destruc-
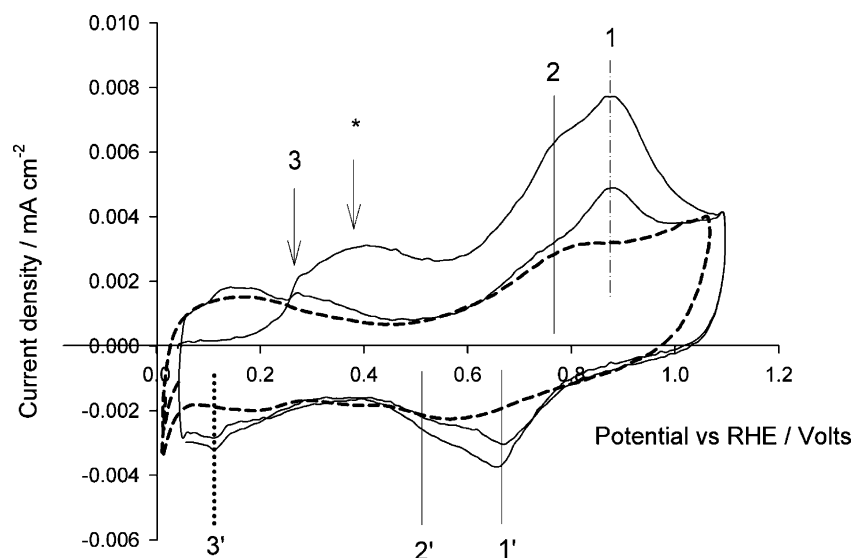
Fig. 5. Cyclic voltammogram of the Pt(1 1 1)–Sn($\sqrt{3} \times \sqrt{3}$)R30° in 0.5 M H_2SO_4 cycled to oxidative potentials (ca. >1.0 V_{RHE}) in the presence of adsorbed CO (solid line, first and second scan) and absence of CO (dotted line, first scan). Each CV was performed on a freshly prepared alloy surface in an independent transfer experiment to ensure that the surface alloy was undisturbed. $1/1'$, $2/2'$ and $3/3'$ are surface redox processes, and '*' is the CO stripping peak.

tion of the surface alloy. This results from the further oxidation of the surface Sn atoms which can eventually move into solution as Sn^{4+}. Fig. 5 shows the first cycle of the CV of the Pt(1 1 1)–Sn($\sqrt{3} \times \sqrt{3}$)R30° surface in 0.5 M H_2SO_4 electrolyte, where the maximum potential was ca. 1.0 V_{RHE} (dotted curve). The low potential redox couple associated with OH adsorption/desorption is absent because of a slightly less well ordered alloy surface. A second surface redox couple is observed at 0.8 V_{RHE}/0.58 V_{RHE}. This is close in potential to a surface redox couple (0.85 V_{RHE}/0.55 V_{RHE}) observed in H_2SO_4 electrolyte for Sn modified Pt(1 1 1) [30], where the Sn was deposited from $SnSO_4$ in H_2SO_4 electrolyte. Repetitive cycling resulted in the destruction of this redox couple. Similar experiments [44] on Sn modified Pt(1 1 1) reveal a redox couple at slightly lower potential (0.60 V_{RHE}/0.55 V_{RHE}); and in this case, it was associated with OH adsorption/desorption. Our results show that partial oxidation of the Sn sites of an alloy take place at lower potential (0.28 V_{RHE}/0.15 V_{RHE}) and we associate the surface redox couple at 0.8 V_{RHE}/0.58 V_{RHE} (Fig. 5) to further oxidation of the Sn sites.

Also shown in Fig. 5 is the first and second cycle to ca. 1.0 V_{RHE} of a well ordered Pt(1 1 1)–Sn($\sqrt{3} \times \sqrt{3}$)R30° surface in 0.5 M H_2SO_4 electrolyte after CO adsorption at 0.05 V_{RHE}. The oxidative stripping of the CO is observed at ca. 0.4 V_{RHE}, will be discussed in detail below. Comparison of the CV in the absence of adsorbed CO (dotted curve) and those following CO stripping (solid curves) shows that the adsorption of the CO significantly influences the surface redox behaviour of the surface. Two surface redox features are observed in the first and second anodic scan, at 0.78 V_{RHE} (2) and at 0.9 V_{RHE} (1), with a corresponding surface reduction peaks in the cathodic cycle at 0.56 V (2′) and 0.70 V (1′), respectively. The persistence of the peaks in the anodic scan

in the second sweep, and the observation of the corresponding reduction peaks provide evidence that these features are not associated with the stripping of adsorbed CO, supporting our conclusion that all CO is stripped in the peak at lower potential [34]. We tentatively suggest that the presence of CO at lower potentials influences subsequent surface redox behaviour by excluding specific adsorption of sulphate anions. The result is that subsequent oxidation of the Sn is more facile, resulting in the new surface redox behaviour. Clearly such a suggestion must be investigated more thoroughly, since one may expect a dependence on the sweep rate in the voltammetry which has not been carried out in this investigation. The suggestion, however, is consistent with results in the literature which indicate that sulphate adsorption is known to influence the surface redox behaviour of Sn modified Pt(1 1 1) surfaces [45,46]. The change in the intensity of the peaks from first to second cycle is evidence of oxidative dissolution of the Sn from the alloy surface under these conditions, a conclusion which will be supported by CO stripping experiments to increasingly high potential in CO saturated solution.

3.3. CO electro-oxidation on the Pt/Sn alloy

The Pt(1 1 1)–Sn(2×2) and Pt(1 1 1)–Sn($\sqrt{3} \times \sqrt{3}$)R30° surfaces were transferred from UHV and exposed to CO contained in a CO saturated 0.5 M H_2SO_4 solution at 0.05 V_{RHE}. The surface was exposed to the CO for sufficient time (5 min) to ensure that the surface (exclusively the Pt sites [25]) was saturated. The electrolyte was then replaced with CO free 0.5 M H_2SO_4, and CO stripping voltammetry carried out (Fig. 6) in the potential range corresponding to the Sn alloy redox behaviour (Fig. 2) and up to 0.5 V_{RHE}. The upper potential limit was chosen because of the further oxi-
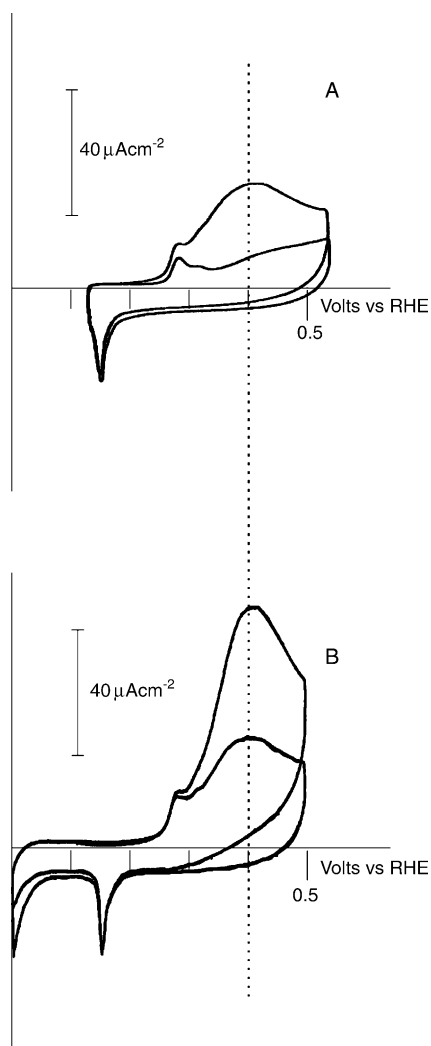
both structures [28]. One may have expected that dosing at room temperature in the electrolyte at higher effective pressures may have given similar coverages to those observed at low temperature, as found for Pt(1 1 1). However, alloying the Pt(1 1 1) surface with Sn results in a significant reduction in the CO desorption temperature (viz. 450 K on Pt(1 1 1) to 339 K on Pt(1 1 1)–Sn($\sqrt{3} \times \sqrt{3}$)R30°), and this may result in lower saturation coverages at room temperature on the Pt(1 1 1)–Sn(2 × 2) and Pt(1 1 1)–Sn($\sqrt{3} \times \sqrt{3}$)R30° surfaces. There is an underlying increase in current in the anodic scan (Figs. 2, 3 and 6) above ca. $0.4\,V_{RHE}$ that is observed after CO is stripped, and in the absence of CO. This is due to the onset of further oxidation of Sn in the alloy (Fig. 5). It will be shown that the presence of the CO on the surface, and its oxidative stripping, appears to modify the surface redox behaviour of the alloyed Sn at higher potentials.

The coincident onset of the CO electro-oxidation with the Sn oxidation (Fig. 6) on the alloy surface is the first time the operation of bi-functional mechanism has been observed unambiguously. Such a mechanism is generally accepted for the Pt/Ru system [7,8,47–50], however there is no corresponding surface redox process associated with the provision of the oxidant by the ruthenium that can be identified on the CO free surface. It appears that the charge associated with the activation of the water to provide the surface adsorbed oxidant is generally very small, as evidenced by the very small currents associated with the process on the Pt(1 1 1)–Sn alloy surfaces. In the case of Sn ad-atoms on platinum, it was indeed suggested on the basis of the redox behaviour at higher potentials ($0.70\,V_{RHE}/0.55\,V_{RHE}$) that Sn could promote the higher equilibrium coverages of oxygen, and correlation with CO oxidation behaviour was consistent with the bi-functional mechanism [51,52]. It is, however, clear from these results that in the case of the Sn alloy surface that OH adsorption takes place at significantly lower potentials, and it is the correspondence of this process directly with CO oxidation which provides direct evidence of such a mechanism.

Fig. 5 includes a CO stripping CV to a higher potential (ca. $1.0\,V_{RHE}$) in CO free, $0.5\,M\,H_2SO_4$ electrolyte on the Pt(1 1 1)–($\sqrt{3} \times \sqrt{3}$)R30° Sn alloy surface. CO is completely stripped in the first cycle in the peak at ca. $0.4\,V_{RHE}$, and as in the limited range sweep exhibits an onset concomitant with the adsorption of OH ($0.28\,V_{RHE}$). Peaks 1/1′ and 2,2′ are associated with the further surface redox behaviour of the alloy surface, as described above. The second cycle shows recovery of the hydrogen UPD structure, and the persistence at lower intensity of the two surface redox features 1,1′ and 2,2′. Already, in the second sweep, there is some degradation of the surface redox couple associated with OH adsorption at $0.28\,V_{RHE}/0.15\,V_{RHE}$ as a result of some disruption of the alloy structure by cycling to higher potentials.

The observed over-potential for CO electro-oxidation (and the peak potential) is considerably lower than bare platinum (by 0.4 V) and ruthenium modified Pt(1 1 1) (by 0.2 V) [9,53] suggesting that well alloyed Pt/Sn catalysts may provide excellent CO-tolerant electrodes. The result is consistent with

Fig. 6. CO stripping volammograms of saturated overlayers of CO on Pt(1 1 1)–Sn(2 × 2) (A) and Pt(1 1 1)–Sn($\sqrt{3} \times \sqrt{3}$)R30° (B) surfaces in $0.5\,M\,H_2SO_4$. The scan rate was $100\,mV\,s^{-1}$. CO was adsorbed from a CO saturated $0.5\,M\,H_2SO_4$ solution under potential control ($0.05\,V_{RHE}$), and the CO stripped in CO free electrolyte.

dation of Sn at higher potentials potentially leading to oxidative dissolution of the Sn component. The over-potential for CO electro-oxidation on Pt(1 1 1) under these conditions is $0.8\,V_{RHE}$ [9]. The first scan of the CV shows a broad oxidation peak at $0.4\,V_{RHE}$, with an onset coincident with the Sn oxidation peak at $0.28\,V_{RHE}$. This corresponds to the oxidation of the adsorbed CO. The second scan shows that nearly the entire CO over-layer on the surface was oxidised in the first sweep. Complete stripping was only hindered by the restriction of the upper potential limit. The coverages of CO on the Pt(1 1 1)–Sn(2 × 2) and Pt(1 1 1)–Sn($\sqrt{3} \times \sqrt{3}$)R30° surfaces, estimated from the associated stripping charges, were $0.37 \pm 0.05\,ML$ and $0.2 \pm 0.05\,ML$. This is about half the saturation coverages observed for CO adsorption at low temperature (150 K) on the same alloy surfaces in UHV, and corresponds to about one CO molecule for every two Pt atoms in the surface layer for

the observation that steady state CO oxidation is strongly promoted by Pt/Sn [24,54]. The onset of CO steady state oxidation indeed coincides with the OH adsorption potential of 0.28 V_{RHE} (Fig. 2). The ability of the Sn atoms to catalyse the oxidation of CO raises the question of the potential activity of the alloy for methanol oxidation, since it is the CO poisoning under steady state methanol oxidation that limits the activity of pure platinum. There was some suggestion that the PtSn alloy is active for methanol oxidation [19,20,55] although it appears that any promotion may have been a result of a solution Sn redox couple [23]. The absence of any promotional effect of Sn in Pt_3Sn alloy surfaces [25] was explained [23] by the presence of a second CO species which was oxidised at higher potentials. We contend that for a well ordered alloy surface, complete stripping of the CO on the small Pt ensembles of the alloy surfaces takes place at the low over-potential (Figs. 5 and 6) as a result of the activation of water on the neighbouring Sn sites (Fig. 2). We further show that oxidation of adsorbed CO at higher potentials takes place only on disordered surfaces when the alloyed Sn is oxidatively stripped from the Pt(1 1 1)–Sn alloy surfaces. The potential of the alloy surfaces for CO-tolerant catalysts, or catalysts for methanol oxidation, appear therefore to hinge on the activity of the small platinum ensembles to oxidise hydrogen or methanol respectively. In order to ensure activity of such a catalyst, however, we show that the surface is susceptible to oxidative modification at potentials ca. >0.5 V_{RHE}.

3.4. Surface alloy stability

To investigate the stability of the ordered alloy surfaces with respect to potential, a series of CO stripping experiments were carried out on the same Pt(1 1 1)–(2 × 2) Sn alloy surface in CO free, 0.5 M H_2SO_4, incrementally increasing the maximum potential of the scan in the range $0.7 < V_{RHE} < 1.10$. The results are shown in Fig. 7. In each case, only the first anodic sweep is shown for clarity (except for the result cycling to 1.1 V_{RHE}, where the second cycle is also included). If the maximum potential is kept below ca. 0.7 V_{RHE}, the CO oxidation behaviour of the ordered alloy surface is observed (Fig. 6), with the onset concomitant with the first OH adsorption at 0.28 V_{RHE}. As the end potential is increased to 1.0 V_{RHE}, the redox associated with the OH adsorption at 0.28 V disappears, and the onset of CO oxidation in the low potential region begins to increase slightly. At the highest end potentials, in addition to the additional redox behaviour of the alloy surface observed above 0.6 V_{RHE} (Fig. 5), CO stripping is observed to develop at ca. 0.75 V_{RHE}. The contribution of CO stripping in two peaks at 0.4 V_{RHE} and 0.74 V_{RHE} on the final surface is highlighted by comparing the first and second scans of the last CV. As one may expect, all the CO has been oxidatively stripped in the first sweep as indicated by the recovery of the hydrogen UPD structure in the second scan.

Comparison of the hydrogen UPD region in the final scan with that characteristic of the well ordered alloy surface
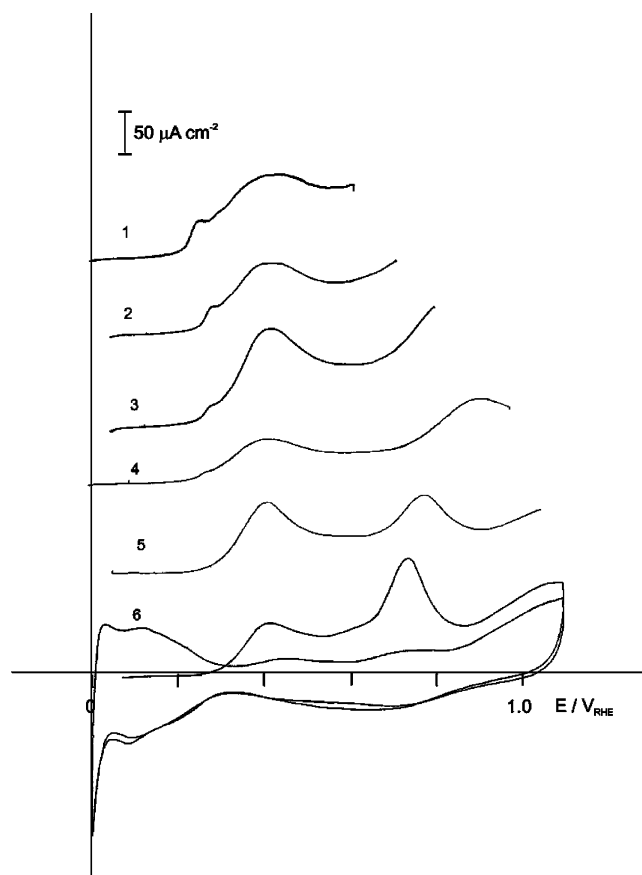

Fig. 7. The first anodic stripping sweep of the stripping voltammograms in a potential window experiment to investigate alloy stability. CO was adsorbed from a CO saturated 0.5 M H_2SO_4 solution under potential control (0.05 V_{RHE}), and the CO stripped in CO free electrolyte. The upper potentials were: (1) 0.70 V_{RHE}; (2) 0.75 V_{RHE}; (3) 0.80 V_{RHE}; (4) 0.95 V_{RHE}; (5) 1.05 V_{RHE}; (6) 1.10 V_{RHE}.

(Fig. 2) clearly indicates that the surface structure has been modified by the increasing anodic potentials. We suggest that the ordered Pt(1 1 1)–(2 × 2) Sn alloy surface has been disrupted by the oxidative dissolution of Sn in one of the two redox peaks (1 or 2 in Fig. 5). Some reductive re-deposition of the Sn takes place in the corresponding reduction peaks (1′ or 2′). The result is a more disordered Pt(1 1 1) surface with islands of adsorbed Sn. CO oxidation at 0.4 V_{RHE} is increasingly dominated by promotion of oxidation by the Sn islands, and at 0.74 V_{RHE} is the oxidation of CO adsorbed on the Pt(1 1 1) disordered surface, far from the Sn islands. The bi-functional activity is therefore effective for CO adsorbed in the remaining regions of the disordering alloy, or at the edges of the re-deposited Sn islands. The fact that there is no longer any clear evidence for the concomitant adsorption of OH (Fig. 7) underlies the importance of order in the surface alloy in observing the small charge associated with OH adsorption. The resulting splitting of the CO oxidation on such a surface is similar to that observed on Pt(1 1 1)–Ru [47] where a similar model has been used to explain the behaviour. What is apparent from the results presented in Fig. 7
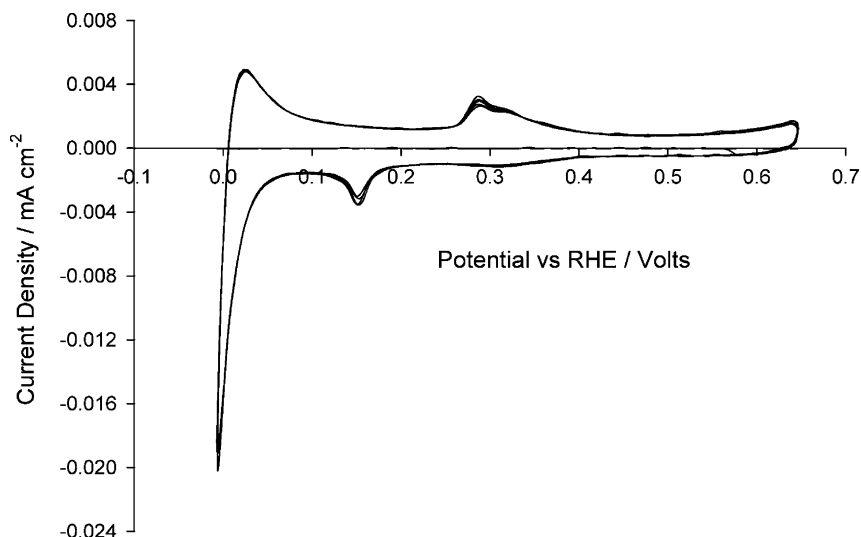
Fig. 8. Cyclic voltammogram of Pt(1 1 1)–Sn($\sqrt{3} \times \sqrt{3}$)R30° in 0.5 M H$_2$SO$_4$ with the potential extended cathodically to induce hydrogen evolution and the subsequent re-oxidation of hydrogen on the surface alloy.

is that the ordered surface alloy is destroyed at anodic potentials above ca. 0.7 V$_{RHE}$, at least in the case where CO has been adsorbed on the surface. Similar window opening experiments carried out on the Pt(1 1 1)–($\sqrt{3} \times \sqrt{3}$)R30° Sn alloy surface in 0.5 M H$_2$SO$_4$ saturated with CO also show a conversion of the CO oxidation behaviour from the ordered alloy surface to a disordered Pt(1 1 1) surface modified by islands of Sn [56] (Fig. 8).

3.5. Hydrogen oxidation on Pt/Sn surface alloys

The activity of the Pt/Sn alloy surface in the electro-oxidation of hydrogen is clearly an important consideration as an anode catalyst in PEMFC. Hydrogen does not dissociatively adsorb from the gas phase on the Pt(1 1 1)–Sn alloy surfaces [28] as a result of a considerably increased barrier to direct dissociation over Pt(1 1 1) [57]. On the other hand, it has been reported [25] that hydrogen oxidation is sustained on the surface of the Pt$_3$Sn(1 1 0) surface. It is evident from the voltammetry in H$_2$SO$_4$ that hydrogen UPD appears to take place on the alloy surfaces (Fig. 2). In order to assess the activity of the alloy surface to molecular hydrogen oxidation, and experiment was carried out on the Pt(1 1 1)–Sn($\sqrt{3} \times \sqrt{3}$)R30° surface in which the potential was cycled to more negative potentials in order to generate hydrogen in the vicinity of the surface in the anodic scan. The upper potential was again restricted in order to assure the integrity of the ordered alloy surface. The redox couple associated with OH adsorption/desorption is observed as expected at 0.28 V$_{RHE}$/0.17 V$_{RHE}$ (Fig. 8). Current is observed in the cathodic scan due to water reduction and concomitant hydrogen evolution at 0.0 V$_{RHE}$. In the subsequent anodic scan, the oxidation of a proportion of the evolved hydrogen is observed at 0.1 V$_{RHE}$, the same as would be observed on

the Pt(1 1 1) surface. No quantitative detail concerning the rate of hydrogen oxidation is available from such measurements; however, it is evident that the surface is reasonably active to hydrogen oxidation, in agreement with the observations on the Pt$_3$Sn(1 1 0) surface [25]. Taken together with the result that CO oxidation is promoted at very low potentials and that CO adsorption is weaker on the Sn alloy than on Pt(1 1 1), with concomitantly lower coverages per platinum site at room temperature.

4. Conclusions

The Pt(1 1 1)–Sn(2 × 2) and Pt(1 1 1)–Sn($\sqrt{3} \times \sqrt{3}$)R30° surfaces have been prepared and characterised in UHV by vapour deposition of Sn on Pt(1 1 1). Surfaces have subsequently been transferred for electrochemical investigation.

A surface redox couple, which is associated with the adsorption/desorption of hydroxide on the Sn sites, is observed at 0.28 V$_{RHE}$/0.15 V$_{RHE}$ in H$_2$SO$_4$ electrolyte on both surfaces. Evidence that it is associated with the adsorption of OH comes from ex situ photoemission measurements, which indicate that the Sn atoms are in a metallic state at potentials below 0.15 V$_{RHE}$, and an oxidised state at potentials above 0.28$_{RHE}$. Specific adsorption of sulphate anions is not associated with the surface process since there is no evidence from photoemission of sulphate adsorption, and the same surface couple is observed in HClO$_4$ electrolyte.

A second surface redox couple, associated with further oxidation of the Sn sites in the alloy surfaces, is observed at 0.8 V$_{RHE}$/0.58 V$_{RHE}$. The redox behaviour at higher potentials is modified by the presence of CO in stripping experiments, with couples now observed at 0.78 V$_{RHE}$/0.56 V$_{RHE}$, and 0.9 V$_{RHE}$/0.70 V$_{RHE}$. This behaviour may be associated

with enhanced oxidation through the exclusion of sulphate anions at the surface by CO.

CO is adsorbed from solution at 300 K, with saturation coverages of 0.37 ± 0.05 ML and 0.2 ± 0.05 ML, respectively. The adsorbed CO is oxidatively stripped at the potential coincident with the adsorption of hydroxide on the tin sites at the lower potential of $0.28\,V_{RHE}$. This strong promotional effect is unambiguously associated with the bifunctional mechanism. The Sn induced activation of water, and promotion of CO electro-oxidation, is sustained as long as the alloy structure remains intact, in the potential range below $0.5\,V_{RHE}$. The instability of the alloy surface at higher potentials is associated with the second redox couple(s). The alloy surface appears to retain activity for the oxidation of hydrogen, and the main disadvantage of the Pt/Sn surface as an anode catalyst in PEMFC is mainly associated with its instability with respect to uncontrolled excursion to anodic potentials.

Acknowledgements

References

[1] D.A.J. Rand, B.D. McNicol, K.R. Williams, J. Power Sources 100 (2001) 47–59.
[2] S. Srinivasan, P. Costamagna, J. Power Sources 102 (2001) 242–252.
[3] S. Wasmus, A. Kuver, J. Electroanal. Chem. 461 (1999) 14–31.
[4] H.A. Gasteiger, N. Markovic, P.N. Ross, E.J. Cairns, J. Phys. Chem. 98 (1994) 617.
[5] H.A. Gasteiger, N.M. Markovic, P.N. Ross, J. Phys. Chem. 99 (1995) 8290–8301.
[6] H.A. Gasteiger, N.M. Markovic, P.N. Ross, J. Phys. Chem. 99 (1995) 16757–16767.
[7] J.C. Davies, B.E. Hayden, D.J. Pegg, Electrochim. Acta 44 (1998) 1181–1190.
[8] J.C. Davies, B.E. Hayden, D.J. Pegg, Surf. Sci. 467 (2000) 118–130.
[9] J.C. Davies, B.E. Hayden, D.J. Pegg, M.E. Rendall, Surf. Sci. 496 (2002) 110–120.
[10] G.-Q. Lu P. Waszczuk, A. Wieckowski, C. Lu, C. Rice, R.I. Masel, Electrochim. Acta 47 (2002) 3637–3652.
[11] B.E. Hayden, in: A. Wieckowski (Ed.), Catalysis and Electrocatalysis at Nanoparticle Surfaces, Marcell Dekker, New York, 2002.
[12] K.P. Geyzers, K.A. Friedrich, A.J. Dickinson, U. Stimming, J. Electroanal. Chem. 524–525 (2002) 261–272.
[13] M.T.M. Koper, J.J. Lukkien, A.P.J. Jansen, R.A. vanSanten, J. Phys. Chem. B 103 (1999) 5522–5529.
[14] M.T.M. Koper, N.P. Lebedeva, C.G.M. Hermse, J. Chem. Soc. Faraday Diss. 121 (2002) 301–311.
[15] E. Christoffersen, P. Liu, A. Ruban, H.L. Skriver, J.K. Norskov, J. Catal. 199 (2001) 123–131.
[16] T.E. Shubina, M.T.M. Koper, Electrochim. Acta 47 (2002) 3621–3628.

[17] M.T.M. Koper, T.E. Shubina, R.A. vanSanten, J. Phys. Chem. B 106 (2002) 686–692.
[18] M.M.P. Janssen, J. Moolhuysen, Electrochim. Acta 21 (1976) 861–868.
[19] M.M.P. Janssen, J. Moolhuysen, J. Catal. 46 (1977) 289–296.
[20] M.A.A. Rahim, M.W. Khalil, H.B. Hassan, J. Appl. Electrochem. 30 (2000) 1151–1155.
[21] E. Grantscharova-Anderson, A.B. Anderson, Electrochim. Acta 44 (1999) 4543.
[22] N.M. Markovic, A. Widelov, P.N. Ross, O.R. Monteiro, I.G. Brown, Catal. Lett. 43 (1997) 161–166.
[23] K. Wang, H.A. Gasteiger, N.M. Markovic, P.N. Ross, Electrochim. Acta 41 (1996) 2587–2593.
[24] H.A. Gasteiger, N.M. Markovic, P.N. Ross, Catal. Lett. 36 (1996) 1–8.
[25] H.A. Gasteiger, N.M. Markovic, P.N. Ross, J. Phys. Chem. 99 (1995) 8945–8949.
[26] A.N. Haner, P.N. Ross, J. Phys. Chem. 95 (1991) 3740–3746.
[27] S. Tillmann, X. Xiao, H. Baltruschat, Phys. Chem. Chem. Phys. 4 (2002) 4044–4050.
[28] M.T. Paffett, S.C. Gebhard, R.G. Windham, B.E. Koel, J. Phys. Chem. 94 (1990) 6831–6839.
[29] H. Wang, H. Massong, G. Samjeske, H. Baltruschat, Electrochim. Acta 46 (2000) 701–707.
[30] S.A. Campbell, R. Parsons, J. Chem. Soc. Faraday Trans. 88 (1992) 833.
[31] P.N. Ross, A.N. Haner, J. Phys. Chem. 95 (1991) 3740–3746.
[32] M.T. Paffett, R.G. Windham, Surf. Sci. 208 (1989) 34–54.
[33] C. Xu, B.E. Koel, M.T. Paffett, Langmuir 10 (1994) 166–171.
[34] B.E. Hayden, M.E. Rendall, O. South, J. Am. Chem. Soc. 125 (2003) 7738–7742.
[35] V.R. Stamenkovic, M. Arenz, C.A. Lucas, M.E. Gallagher, P.N. Ross, N.M. Markovic, J. Am. Chem. Soc. 125 (2003) 2736–2745.
[36] B.E. Hayden, A.J. Murray, R. Parsons, D.J. Pegg, J. Electroanal. Chem. 409 (1996) 51–63.
[37] B.E. Hayden, in: A. Wieckowski, E.R. Savinova, C.J. Vayenas (Eds.), Catalysis and Electrocatalysis at Nanoparticle Surfaces, Marcel Dekker, New York, 2003, pp. 171–210.
[38] D. Briggs, M. Seah, Practical Surface Analysis by Auger and X-ray Photoelectron Spectroscopy, John Wiley & Sons Ltd., Chichester, 1983.
[39] S.H. Overbury, D.R. Mullins, M.T. Paffett, B.E. Koel, Surf. Sci. 254 (1991) 45–57.
[40] J. Clavilier, J. Electroanal. Chem. 107 (1980) 211–216.
[41] A. Logadottir, P. Liu, J.K. Norskov, Electrochim. Acta 48 (2003) 3731–3742.
[42] Z. Shi, J. Lipkowski, J. Electroanal. Chem. 364 (1994) 289–294.
[43] N. Markovic, P.N. Ross, Langmuir 9 (1993) 580–590.
[44] S. Tillmann, H. Massong, T. Langkau, E.A. Abd El Meguid, H. Baltruschat, Electrochim. Acta 44 (1998) 1379–1388.
[45] X.-Y. Xiao, S. Tillmann, H. Baltruschat, Phys. Chem. Chem. Phys. 4 (2002) 4044–4050.
[46] H. Massong, S. Tillmann, T. Langkau, E.A. Abd El Meguid, H. Baltruschat, Electrochim. Acta 44 (1998) 1379–1388.
[47] J.C. Davies, B.E. Hayden, D.J. Pegg, M.E. Rendall, Surf. Sci. 496 (2002) 110–120.
[48] M. Watanabe, S. Motoo, J. Electroanal. Chem. 60 (1975) 267.
[49] M. Watanabe, S. Motoo, Electroanal. Chem. Interfacial Electrochem. 60 (1975) 275–283.
[50] N.P. Lebedeva, M.T.M. Koper, J.M. Feliu, R.A. van Santen, J. Electroanal. Chem. 524 (2002) 242–251.
[51] M. Shibata, M. Watanabe, S. Motoo, J. Electroanal. Chem. 187 (1985) 161–174.
[52] M. Watanabe, S. Motoo, J. Electroanal. Chem. 69 (1976) 429–431.
[53] W. Chrzanowski, A. Wieckowski, Langmuir 13 (1997) 5974–5978.

[54] H.A. Gasteiger, N.M. Markovic, P.N. Ross, In: Report "On the differences in the reaction mechanism for CO and CO/H_2 electrooxidation on PtRu and PtSn Alloy Electrodes.", *Materials Sciences Division, Berkeley National Laboratory*. Report No. LBNL-40196, UC-1501. April 1997.

[55] T. Frelink, W. Visscher, J.A.R. Vanveen, Surf. Sci. 335 (1995) 353–360.

[56] M.E. Rendall, In: Thesis: "The modification of platinum single crystals for fuel cell electrocatalysis. A UHV and electrochemical study.", *School of Chemistry, Department of Science and Engineering*; University of Southampton: Southampton, 2003, p 185.

[57] P. Samson, A. Nesbitt, B.E. Koel, A. Hodgson, J. Chem. Phys. 109 (1998) 3255–3264.